Strategic Regions for Monitoring Incoming Low-Energy Transfers to Low-Lunar Orbits

Yuri Shimane, Kento Tomita, and Koki Ho
Georgia Institute of Technology

ABSTRACT

Low-energy transfers (LETs) are attractive translunar trajectories with typically lower lunar orbit insertion costs than direct transfers. With the expected increase in traffic on LETs by both government and commercial players alike, a key part of space situational awareness activity in cislunar space will involve monitoring incoming spacecraft on these transfers. To address this requirement, a facility location problem is formulated to obtain the optimal number and locations where observer spacecraft should be placed, along with monitoring allocations at specific times to specific regions in cislunar space. The observers are tasked to monitor for clustered families of LETs to low-luna orbit (LLO), constructed from a database of LETs in the bi-circular restricted four-body problem.

1. INTRODUCTION

Low-energy transfers (LETs), also called ballistic lunar transfers (BLTs), are a class of translunar trajectories that leverage the third-body effect of the Sun to its advantage to reduce the arrival ΔV cost in cislunar space [21, 26]. In exchange, LETs require longer times of flight typically ranging around 3 months. This makes LETs unsuitable for crewed campaigns, but they are still attractive for robotic lunar missions. While the history of spacecraft flying along a LET goes back to JAXA's Hiten mission in 1991 [21] and NASA's GRAIL mission [29] in 2011, the use of LETs in frequent years between flown and planned missions have dramatically increased; in 2022 alone, NASA's CAPSTONE mission [6], KARI's Danuri mission [19], and ispace's M1 mission [20] all utilized LETs. Among the multiple NASA Commercial Lunar Payload Service (CLPS) missions planned over the next few years together with the roll-out of more Artemis missions, the traffic along LETs to cislunar space is expected to grow rapidly.

With the increase in cislunar activities by both commercial and governmental players, interest in cislunar space domain awareness (SDA) has also seen a significant increase; several studies have considered both monitoring vast cislunar regions [1, 4, 10, 13, 14, 16, 35, 36], as well as tracking specific translunar and cislunar trajectories of interest [12, 15, 34]. In particular, Wilmer et al [38, 39] and Dahlke et al [11] studied the use of libration point orbits (LPOs) for monitoring targets also located in L1 and L2 LPOs; notably, Wilmer and Bettinger [38] looked at monitoring the near-rectilinear halo orbit (NRHO), which is the planned hosting orbit for the Lunar Gateway.

Meanwhile, monitoring for a priori unknown, incoming LETs is a substantially different cislunar SDA problem; the high apogee of LETs, typically in the range of 1.5 million km, is far beyond the so-called xGEO region [25] considered for SDA. Aside from the technical difficulty, observing these remote regions would also be impractical from a resource point of view for the near future, since the apogee of LETs can vary in locations dramatically, typically lying close to the Sun-Earth L1 or L2 points. Instead, it would be more sensible to monitor for LETs by anticipating their arrival into the lunar vicinity, as they come in from the far side of the Moon. Note that LETs can be used for transfers heading to LPOs as well as to low lunar orbits (LLOs). In the case of going to LPOs, structures such as invariant manifolds or Cauchy-Green tensors may be leveraged in such a way that the spacecraft asymptotically approaches the desired LPO. In such a case, it is likely to be observable from architectures such as the one studied by Wilmer et al [38, 39]. In contrast, with the inherently chaotic nature of the underlying dynamics at play, LETs to LLOs [27] approach the Moon's vicinity through a substantially different and diverse set of possible paths. As both Moon-orbiting and landing missions involve getting to LLOs instead of LPOs, this work focuses on this subset of LETs.

Through this work, we propose an analysis for monitoring spacecraft flying along LETs to LLOs as they approach the Moon's vicinity. We leverage a database of LETs generated in the bicircular restricted four-body problem (BCR4BP) and prune the trajectories based on mission operations criteria to identify a subset of LETs that are most likely to be flown frequently. Then, leveraging the periodic nature of LET launch windows, an optimization problem to

identify the optimum number and location(s) for observer spacecraft of the LET monitoring architecture is solved. The optimization problem is formulated as a facility location problem (FLP) from the operations research literature [8, 9, 18, 30, 32, 40]. The FLP is a class of optimization problems that aims at finding the optimal location and number of facilities to meet the demands of a set of clients. In the context of monitoring LETs, the facility is the observer spacecraft, and the clients' "demand" corresponds to an observation requirement in case a spacecraft flies through the LETs.

This paper is organized as follows: first, in Section 2 preliminaries on the dynamical systems, and more specifically the bicircular-restricted four-body problem (BCR4BP), are introduced. This is followed in Section 3 by a discussion on LETs to LLOs, with a particular focus on their characteristics that relate to monitoring them. In Section 4, the observation model that is employed to study the monitoring architecture is introduced. Then, 5 introduces the facility location problem applied to this scenario. Section 6 shows the results found from the proposed approach. Finally, conclusive remarks are provided in Section 7.

2. DYNAMICAL SYSTEMS PRELIMINARIES

Various classes of restricted three-body problems offer useful dynamical frameworks for studying motions in the Earth-Moon system. In particular, the CR3BP and the BCR4BP models are introduced. The former is the basis for the latter model, which is particularly useful for considering LETs in a simplified model, due to the presence of the Earth, Moon, and Sun as bodies exerting force on the spacecraft. Beyond the context of translunar and cislunar trajectory design, the BCR4BP has also been applied to simulating cislunar SDA by Bhadauria and Frueh [3] as it incorporates the Sun, which is the illuminating source, into the dynamics.

In this work, while the observer spacecraft's dynamics are modeled using the CR3BP, the LETs are modeled using the BCR4BP. This hybrid choice of dynamical models is further discussed in Section 4.1. In this Section, the CR3BP and BCR4BP are introduced, and the hybrid choice of dynamical models is further discussed in Section 4.1.

2.1 Circular Restricted Three-Body Problem

The CR3BP equations of motion are given by

$$\ddot{x} - 2\dot{y} = \frac{\partial U}{\partial x}\,,\ \ddot{y} + 2\dot{x} = \frac{\partial U}{\partial y}\,,\ \ddot{z} = \frac{\partial U}{\partial z} \tag{1}$$

where U is the pseudo-potential of the CR3BP system, given by

$$U = \frac{x^2+y^2}{2} + \frac{1-\mu}{r_1} + \frac{\mu}{r_2} \tag{2}$$

where $\mu = M_2/(M_1+M_2)$ is the mass ratio, r_1 is the distance to M_1, and r_2 is the distance to M_2, given by

$$r_1 = \sqrt{(x+\mu)^2+y^2+z^2} \tag{3}$$

$$r_2 = \sqrt{(x-1+\mu)^2+y^2+z^2} \tag{4}$$

In the context of the Earth-Moon system, M_1 corresponds to the Earth and M_2 corresponds to the Moon. The state-transition matrix $\Phi(t)$ is propagated through the Jacobian of the dynamics

$$\dot{\Phi}(t) = A(t)\Phi(t) = \left[\begin{array}{c|c} \mathbf{0}_{3,3} & I_{3,3} \\ \hline U_{\boldsymbol{xx}} & 2\boldsymbol{\Omega} \end{array}\right]\Phi(t) \tag{5}$$

where $U_{\boldsymbol{xx}} \in \mathbb{R}^{3\times 3}$ is the second-order partials of U, and

$$\boldsymbol{\Omega} = \begin{bmatrix} 0 & 1 & 0 \\ -1 & 0 & 0 \\ 0 & 0 & 0 \end{bmatrix}$$

Table 1: Parameters of BCR4BP dynamics

Parameter	Value
Earth-Moon system mass parameter μ, n.d.	0.012150584269940354
Canonical length scale LU, km	384400.0
Canonical time scale TU, s	375190.2619517228
Relative mass of the Sun m_s, n.d.	328900.5598102475
Relative distance of the Sun from the Earth-Moon barycenter a_s, LU	389.1779396462019
Angular velocity of the Sun ω_s, rad/TU	-0.9253018261815922

2.1.1 Libration Point Orbits

In the CR3BP, periodic motions exist about primary bodies as well as around the libration points, also known as libration point orbits (LPOs). By definition, a periodic orbit satisfied $\boldsymbol{x}(t+P) = \boldsymbol{x}(t)$ where $\boldsymbol{x}(t) \in \mathbb{R}^6$ is the position and velocity states, and P is the period of the orbit. In this work, we consider LPOs as candidate observer locations due to their advantageous positioning in the vicinity of the neck regions of the Earth-Moon system. For a given periodic orbit, its linear stability metric ν is computed from the maximum eigenvalue of the state-transition matrix Φ over one full period P, $\lambda_{\max} = \max\{\text{spec}(\Phi(P,0))\}$, via the equation

$$\nu = \frac{1}{2}\left|\lambda_{\max} + \frac{1}{\lambda_{\max}}\right| \tag{6}$$

2.2 Bicircular-Restricted Four-Body Problem

In the BCR4BP, the orbital plane of the Sun-Earth system and the Earth-Moon system are commonly assumed to be coplanar [5]; as such, the Sun's motion is represented as a clockwise rotation around the Earth-Moon barycenter on the xy-plane of the Earth-Moon rotating frame. The BCR4BP equations of motion are given by

$$\ddot{x} - 2\dot{y} = \frac{\partial \tilde{U}}{\partial x}\,,\ \ddot{y} + 2\dot{x} = \frac{\partial \tilde{U}}{\partial y}\,,\ \ddot{z} = \frac{\partial \tilde{U}}{\partial z} \tag{7}$$

where $\tilde{U}$ is the pseudo-potential of the BCR4BP system, given by

$$\tilde{U} = U + \frac{m_s}{r_s} - \frac{m_s}{a_s^3}(x_s x + y_s y + z_s z) \tag{8}$$

where

$$m_s = \frac{M_\odot}{M_1 + M_2} \tag{9}$$

$$r_s = \sqrt{(x-x_s)^2 + (y-y_s)^2 + (z-z_s)^2} \tag{10}$$

$$\begin{bmatrix} x_s \\ y_s \\ z_s \end{bmatrix} = a_s \begin{bmatrix} \cos\theta_s(t) \\ \sin\theta_s(t) \\ 0 \end{bmatrix} \tag{11}$$

where $M_\odot$ is the mass of the Sun, θ_s is the Sun angle, which corresponds to the angle between the Sun-direction vector and the Earth-Moon vector, given by

$$\theta_s(t) = \omega_s t + \theta_{s,0} \tag{12}$$

Here, ω_s is the angular velocity of the Sun going around the Earth-Moon barycenter, and $\theta_{s,0}$ is the Sun-direction angle at some initial time. Parameters of the dynamics used in this work are taken from SPICE data and are shown in Table 1. Note that $\omega_s < 0$, hence the Sun appears to revolve clockwise about the Earth-Moon barycenter from an observer in the Earth-Moon rotating frame.

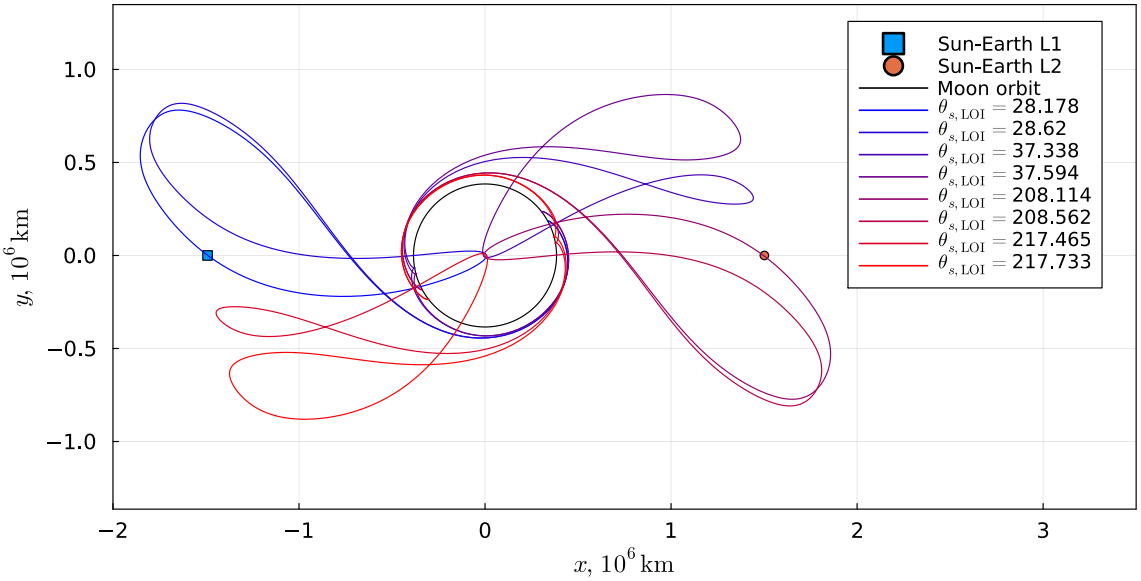

Fig. 1: Example of periodicity exhibited by low-energy transfers, in the Sun-Earth rotating frame centered at Earth

3. LOW-ENERGY TRANSFERS

LETs are a class of translunar transfer that leverages the Sun's gravitational perturbation. Specifically, the perigee of the orbit, which initially coincides with the LEO at which the translunar injection is conducted, is raised to roughly that of the Moon's orbit about the Earth through the Sun's third-body effect. This is a relatively slow effect that takes place (1) slowly, and (2) is most effective far away from the Earth or the Moon. As such, the typical apogee of LETs lies at around 1.5 million km, and the transfer times can span about 90 to 120 days [26]. While this extended time of flight is prohibitive for crewed missions, the ΔV savings obtained in return make LETs attractive for robotic missions, both for exploration and exploitation of the cislunar ecosystem.

From the point of view of SDA activities, it is also noteworthy that the apogee lobe of LETs extends far beyond the Moon's orbit, as shown in Figure 1. As such, it is unrealistic to expect architectures from existing cislunar SDA studies that typically target regions up to Earth-Moon L2 to be able to track a spacecraft all the way along a LET. Meanwhile, it is also likely impractical to place architectures for the sole sake of observing LETs all the way along its path, as these can take diverse geometries, most poignantly due to their vicinity to the boundary of the Earth's sphere of influence around their apogees.

In this work, we construct a database of LETs in the BCR4BP, which is then clustered into families through a combination of Dynamic Time Warping and DBSCAN. This Section initially introduces some characteristics of LETs, followed by a description of this clustering process.

3.1 Periodicities of Launch and Arrival Time Window

There are two periodicities associated with launch and arrival time windows with LETs. At the longer time scale, there is a monthly periodicity for any LET in the BCR4BP, as the Earth, Moon, and Sun come back to the exact same orientation every synodic period. Note that when transitioned to the full-ephemeris model, this relationship becomes only quasi-periodic, as effects of the eccentricities of the Earth-Moon system as well as the inclination difference of the Earth-Moon and Sun-Earth orbital planets, among other minor discrepancies of the dynamics, start to kick in.

The second periodicity occurs at roughly 14.75 days or roughly half of the synodic period. This is due to the fact that the Sun's gravity gradient may be leveraged on both the Sun-Earth L1 or Sun-Earth L2 side to raise the perigee of the spacecraft to the Moon's orbit. Figure 1 exhibits this second periodicity. The 8 transfers shown all share the same perigee at departure and arrive at the exact same LOI state vector, but the Sun angle θ_s at the time of LOI are all different.

3.2 Lunar Orbit Arrival Geometry

In this work, LETs going into 100 km altitude LLOs are considered. We define analogs of RAAN and inclination in the inertially frozen frame as $\tilde{\Omega}$ and $\tilde{i}$; the fictitious RAAN $\tilde{\Omega}$ is the angle between the x-axis of the Earth-Moon rotating plane of the nodal line of the orbital plane in the Keplerian sense at LOI, such that $\tilde{\Omega} = 0^\circ$ corresponds to the ascending node located on the far side of the Moon, and $\tilde{\Omega} = 180^\circ$ corresponds to the ascending node located on the near side of the Moon. The fictitious inclination $\tilde{i}$ is defined as the inclination of the orbital plane in the Keplerian sense at LOI with respect to the Earth-Moon orbital plane, or equivalently the xy-plane of the Earth-Moon rotating frame.

3.3 Clustering Low-Energy Transfers

Given a set of LETs meeting the aforementioned criteria, a clustering method is then applied to separate the LETs into families sharing geometric similarities during their approach phase to LLO. Then, for each family of candidate LETs for future missions, regions of interest for monitoring are defined in the subsequent Section. In order to cluster the trajectories, a scalar metric to quantify the similarity of two trajectories is required. There are a number of different measures that can be metric or non-metric, discrete or continuous, and relative or absolute [33]. In this work, the Dynamic Time Warping (DTW) [2, 7] measure is employed to cluster the database of LETs into families. For the purpose of later using the families as bundles to be monitored from an observer spacecraft, the "distance" between two spacecraft is measured in four-dimensional space, consisting of the separation in position vectors as well as the phase θ_s. Once the DTW between each combinatorial pair of trajectories are computed, the trajectories may be clustered using well-established clustering techniques; in this work, we employ a DBSCAN.

Figure 2 shows the clustered LETs, in a revolving cut-away of the Earth-Moon rotating frame's xy-plane. This illustrates the role the phasing plays in LETs; for example, the departure from the cislunar vicinity, visible by increasing values in y-axis position (in the Earth-Moon rotating frame), is shared between clusters 1 and 3, or clusters 4 and 5, respectively, despite their distinctive structure in the vicinity of the Moon, as seed by the looping structure around the dotted circle corresponding to the Moon's location.

4. SIMULATION OF LET MONITORING ARCHITECTURE

In this Section, the framework to simulate the monitoring activity of LET targets is introduced. We employ a hybrid dynamics model, where the observers are propagated using the CR3BP, while the state history of the LET is obtained using the BCR4BP. Libration point orbits (LPO) are considered for candidate observer locations. The visibility of a target is considered using an approximate expression for the apparent magnitude of an object, and the notion of the minimum-volume visibility sphere is introduced to study the observation of a particular family of LETs at a given time.

4.1 Selection of Dynamical Systems Models

The LET monitoring problem is considered through the use of mixed dynamical models, namely of the CR3BP and the BCR4BP; specifically, the observer locations, which are to be placed on LPOs, are modeled using the CR3BP, while the target spacecraft flying along LETs, which will be discussed in further detail in the subsequent Section, is modeled using the BCR4BP.

These choices have been made due to the following considerations: firstly, for the observer, while the purely periodic orbit does not exist in a full-ephemeris environment, there exists quasi-periodic counterpart orbits that poses sufficiently similar characteristic to the CR3BP periodic motion; this is particularly true for LPOs on some low-integer resonance with the Sun-Earth-Moon's synodic period. Indeed, the idea of using LPOs in the CR3BP to assess the feasibility of these locations in space for SDA activity has been explored in multiple previous works successfully [35, 36]. In contrast, the motion of the targets to be observed, which can evolve independently from the motion of the observers, are specifically transfers that require and leverage the Sun's perturbation. While the motion of the spacecraft within the lunar sphere of influence is affected to a much smaller extent by the presence of the Sun, the target's path is modeled all the way from the departure perigee to the arrival perilune using the BCR4BP for consistency along its path.

4.2 Candidate Observer Periodic Orbits

Previous works by Vendl and Holzinger [35] as well as Visonneau et al [36] have highlighted the utility of well-phased LPOs with resonance to the synodic period due to the repeating pattern of the illumination conditions. In this work,

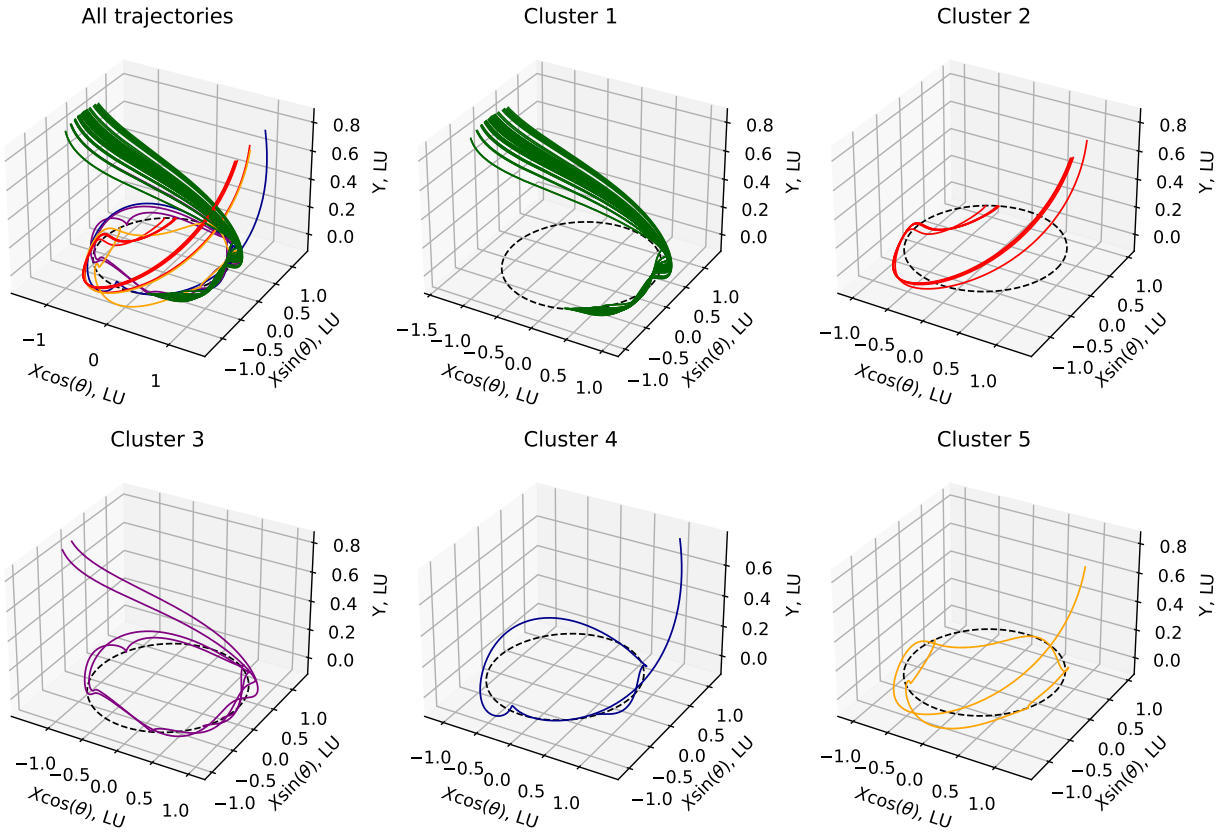

Fig. 2: Clustered low-energy transfers, shown in a revolving cut-away of the Earth-Moon rotating frame's xy-plane. The horizontal plane of each figure shows the polar x-axis position of the spacecraft, while the vertical axis corresponds to its y-axis position.

LPOs in the vicinity of Earth-Moon L2 are prioritized due to their proximity to the outer neck region of the Earth-Moon system. This selection is due to the observation that all LETs pass through this neck region to enter into the vicinity of the Moon. Specifically, resonant members of the L2 Lyapunov and L2 halo orbits are considered. These are shown in Figure 3, and are summarized in Table 2. Note that an M : N resonance indicates the spacecraft completes M revolution during N synodic periods.

4.3 Visibility Modeling

The visibility of an object can be quantified using the apparent magnitude, which is a logarithmic quantity that compares the intensity of an object with respect to another. In this work, we adopt the conservative approximation of apparent magnitude given in Vendl and Holzinger [35]. For a target with diameter d, specular reflectance a_{spec} and diffuse reflectance a_{diff} at a range ζ_T from an observer, its apparent magnitude m is given by

$$m = m_{\odot} - 2.5\log_{10}\left(\frac{d^2}{\zeta_T^2}\left[\frac{a_{\text{spec}}}{4} + a_{\text{diff}}\, p_{\text{diff}}(\psi)\right]\right) \tag{13}$$

where $m_{\odot} = -26.74$ is the apparent magnitude of the Sun, ψ is the solar phase angle given by

$$\psi = \arccos\left(\frac{\boldsymbol{\zeta}_{\text{T}} \cdot \boldsymbol{r}_{\odot\text{T}}}{\|\boldsymbol{\zeta}_{\text{T}}\|\,\|\boldsymbol{r}_{\odot\text{T}}\|}\right) \tag{14}$$

where $\boldsymbol{\zeta}_{\text{T}}$ is the line of sight vector from the observer to the target, $\boldsymbol{r}_{\odot\text{T}}$ is the line of sight vector from the Sun to the target, and p_{diff} is the diffuse phase angle function for a diffuse sphere, given by

$$p_{\text{diff}}(\psi) = \frac{2}{3\pi}[\sin(\psi) + (\pi - \psi)\cos(\psi)] \tag{15}$$

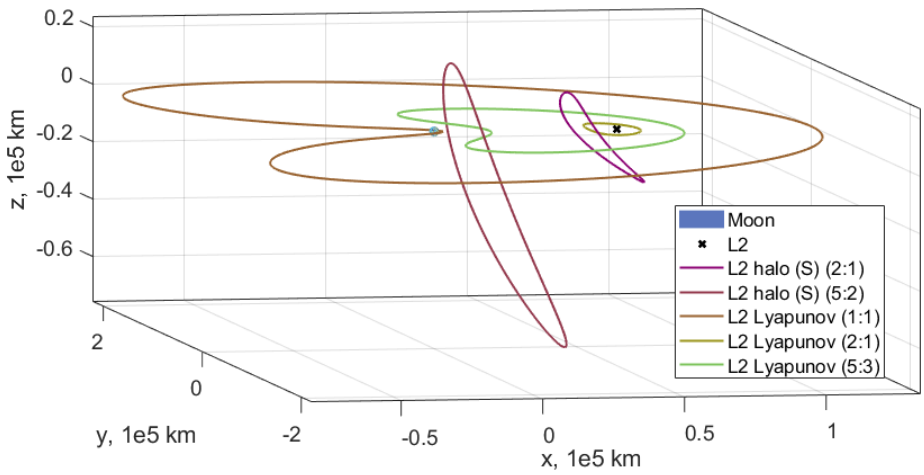

Fig. 3: Candidate libration orbits for observer considered

4.4 Minimum-Volume Visibility Sphere of a Low-Energy Transfer Cluster

For a given set of a cluster LET, at some given time, the states along each LET within the cluster are scattered in some area of the phase space. We consider the minimum enclosing sphere for the positions of these states, which can be found by applying Welzl's algorithm [37], which returns the center of the sphere, denoted hereafter as $\boldsymbol{r}_C$, and the radius, denoted as R_{MVVS}. We refer to this sphere as the minimum-volume visibility sphere (MVVS), as it represents the smallest volume that must be visible to the observer spacecraft in order for any LET state within the cluster to be detectable. Figure 4 illustrates the MVVS for a cluster of LET along with hypothetical spacecraft flying along those LETs, shown by red triangles.

Once the MVVS is formed, let the point that is least visible to the observer, corresponding to the largest apparent magnitude m, be denoted by spatial coordinates (x_m, y_m, z_m) relative to $\boldsymbol{r}_C$. These coordinates can be obtained by solving the constrained optimization problem

$$\begin{aligned} &\max_{x_m, y_m, z_m} \quad m \\ &\text{such that} \quad x_m^2 + y_m^2 + z_m^2 \leq R_{\text{MVVS}}^2 \end{aligned} \tag{16}$$

where (x_0, y_0, z_0) is the center of the MVVS, and R_{MVVS} is its radius. The objective m is calculated as a function of (x_m, y_m, z_m) by computing the line of sight vector $\boldsymbol{\zeta}_T$ to this point, via

$$\boldsymbol{\zeta}_T = \bar{\boldsymbol{\zeta}}_T + \begin{bmatrix} x_m \\ y_m \\ z_m \end{bmatrix} \tag{17}$$

where $\bar{\boldsymbol{\zeta}}_T$ is the line of sight vector to the center of the MVVS, and substituting back into equation (13).

5. OPTIMIZATION PROBLEM

The LET monitoring architecture is designed using the facility location problem (FLP). In particular, the discrete FLP, where the candidate locations for the observer are discretized, is a particularly powerful formulation as it lends the problem into a binary linear program and a globally optimal solution can be obtained. This discretization is non-trivial in the context of space-based assets since spacecraft in space will always be in motion along its orbit. In the context of two-body dynamics, orbital "slots" may be defined by discretizing in orbital elements space [22, 23, 31], while in the context of three-body dynamics, a finite set of periodic orbits may be considered, each with some finite number of "slots" discretized in phase [28]. This Section first introduces the optimization problem, with descriptions of the variables, the objective, and the constraints. The FLP is formulated in discrete space, thus requiring discretization of both space and time; considerations on this process are also discussed.

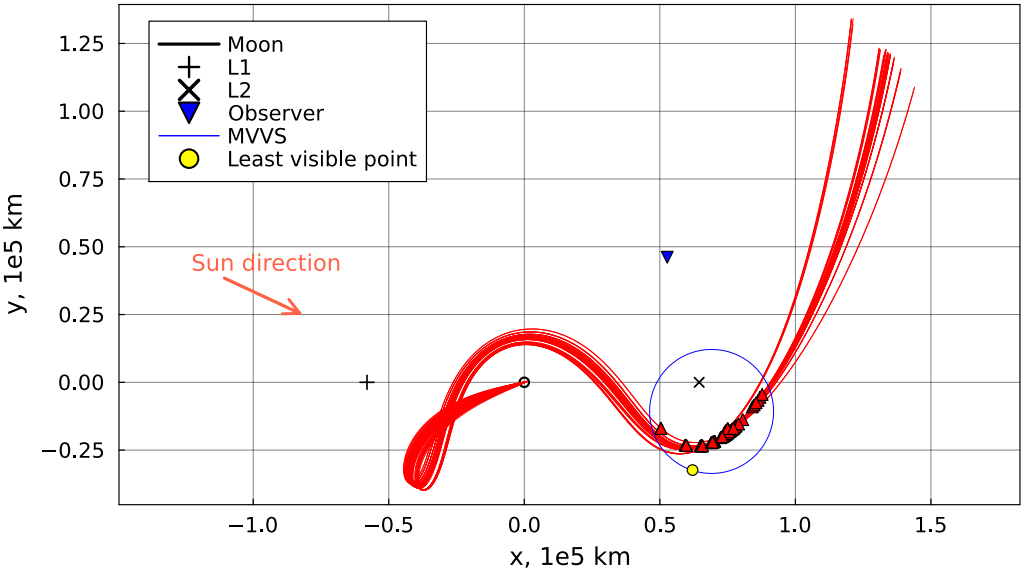

Fig. 4: Example minimum-volume visibility sphere in the Earth-Moon rotating frame centered at the Moon for a cluster of LETs, shown in red lines, where the spacecraft along these LETs at a particular time instance are shown by the red triangles. The yellow circle corresponds to the least visible point (x_m, y_m, z_m) within the MVVS.

5.1 Facility Location Problem for LET Monitoring Architecture

Let the set of candidate observer locations given by $j \in [1,\ldots,n_j]$, targeted clusters of LETs, hereafter denoted as LET sets, given by $i \in [1,\ldots,n_i]$, and time steps given by $t \in [1,\ldots,n_t]$. Furthermore, let the variable $Y \in \mathbb{B}^{n_j}$ denote whether to use the candidate observer location j, and variable $X \in \mathbb{B}^{n_i \times n_j \times n_t}$ denote whether observer j looks at a target MVVS i at time step t. The FLP is given by

$$\min_{X,Y} \sum_j f_j Y_j$$
$$\text{such that} \quad \begin{cases} X, Y \in \{0,1\} \\ \sum_t \sum_j M_{ijt} X_{ijt} = N_{\Delta t} \quad \forall i \\ \sum_i X_{ijt} \leq 1 \quad \forall j,t \\ X_{ijt} \leq Y_j \quad \forall i,j,t \end{cases} \tag{18}$$

where $f_j \in \mathbb{R}^{n_j}$ is the cost associated with observer location j, $M \in \mathbb{B}^{n_i \times n_j \times n_k}$ is a binary matrix dictating whether target i is visible to observer j at time-step t, and $N_{\Delta t}$ is the minimum number time-step during which the LET set must be observed upon approach. We denote M as the visibility matrix hereafter. The problem aims at monitoring the LET with the minimum number of observers. The first constraint simply dictates the variables to be binary. The second constraint ensures that there exists $N_{\Delta t}$ observation instances for all target LET sets. The third constraint ensures that the observer is tasked to observe at most one target LET set at any time, and the last constraint ensures the observation allocation to be used only if the j^{th} observer exists.

5.2 Discretization Schemes

While there is a discrete number of LET sets by construction of the clusters, candidate observer locations, as well as the times at which the LET sets could be observed, are continuous quantities by nature. These must be discretized to accommodate for the problem formulation in (18).

Table 2: Candidate Observer Libration Point Orbit Slots

Libration Point Orbit	Period, day	Synodic resonance	Stability index, ν	Facility cost coefficient f	Number of slots
L2 Halo Southern	14.75	2:1	510.134	0.9981	117
L2 Halo Southern	11.8	5:2	9.105	0.9477	94
L2 Lyapunov	19.5	1:1	49.604	0.9832	234
L2 Lyapunov	14.75	2:1	654.810	0.9985	117
L2 Lyapunov	17.7	5:3	161.353	0.9942	141
				Total	703

5.2.1 Discretization of Observation Times

Since LETs enter the vicinity of the Moon through the neck region at different Sun angle θ_s, the observation times must span over a sufficiently long duration to capture all possible timings where the LET cluster may be visible to the observer. In this work, the observation time-steps range within $\theta_s = [0, 2\pi]$ and is discretized using 200 steps, resulting in a time-step of about 3.03 hours.

5.2.2 Discretization of Observer Locations

Along each candidate periodic orbit given in Table 2, the observer may be placed into any arbitrary phase along the LPO with respect to the Sun angle. Thus, the candidate observer locations consist of "slots" with distinct phase angles along each LPO. Note that this notion of candidate orbital slots is akin to previous works in the literature [22, 23, 28, 31]. Along each LPO, the number of candidate slots that differ in phase are obtained by rounding up the period divided by $\Delta t \approx 3.03$ hours. The resulting number of candidate slots along each orbit are given in Table 2.

5.3 Facility Cost Vector

The cost associated with a specific facility j, stored in the vector f_j, quantifies the relative cost for using a particular observer location. Since all candidate locations are Earth-Moon LPOs, the transfer costs are assumed to be similar; as such, the cost of the observer locations is constructed to reflect the operational cost of placing a spacecraft in a specific orbit, which arises from the station-keeping cost. The expression for f_j is given by

$$f_j = \frac{-1}{\nu_j + 10} + 1 \tag{19}$$

where $\nu_j \in \mathbb{R}$ is the linear stability index of the periodic orbit j, computed from equation (6). Expression (19) is used instead of directly using $f_j = \nu_j$ in order to have a better scaling between the nearly stable ($\nu \approx 1$) and unstable (ν in the order of 100s) periodic orbits as shown in Table 2, as well as having penalizing ($f_j > 0$) values for periodic orbits with $\nu < 1$.

5.4 Visibility Coefficients Matrix

The binary entries of the visibility matrix M is pre-computed ahead of solving the optimization problem (18). This involves checking, for each combination of i, j, and t, if the target MVVS i is visible to observer j. The following conditions must be verified to confirm the visibility:

- the apparent magnitude is below a pre-defined cut-off magnitude, $m \leq m_{\text{co}}$, and
- the observer is not inside the MVVS, and the sector angle of the tightly bounding cone to the MVVS is within a pre-defined field of view (FOV).

The last condition ensures the MVVS falls within the FOV of the observer. If the observer is within the MVVS, a field of view of 360° would be required, hence the MVVS is deemed invisible; if the observer is outside the MVVS, the

sector angle of the tightly bounding cone, denoted as δ, is calculated by

$$\delta = 2\arcsin\left(\frac{R_{\text{MVVS}}}{\bar{l}_T}\right) \tag{20}$$

This condition can be expressed mathematically as

$$M_{ijt} = \begin{cases} 0 & \text{if } \|\boldsymbol{r} - \boldsymbol{r}_C\| \leq R_{\text{MVVS}} \\ 0 & \text{else if } \delta \geq \text{FOV} \\ 0 & \text{else if } m > m_{\text{co}} \\ 1 & \text{otherwise} \end{cases} \tag{21}$$

Algorithm 1 summarizes the process of computing M_{ijt}.

Algorithm 1 Computation of observability coefficients matrix

Require: $n \geq 0$
  for $i = 1 : n_i$ **do**
    for $j = 1 : n_j$ **do**
      for $t = 1 : n_t$ **do**
        $\boldsymbol{l}_T \leftarrow$ solve optimization problem (16)
        $m \leftarrow$ equation (13) ▷ Compute visible magnitude of least visible point state
        $M_{ijt} \leftarrow$ equation (21)
      end for
    end for
  end for

6. NUMERICAL EXPERIMENTS

The proposed method is implemented using the JuMP modeling language [24] in Julia. The least visible point, given by problem (16), is solved by IPOPT [41], and the FLP (18) is solved with Gurobi [17]. In the FLP, an observation time-step requirement of $N_{\Delta t} = 3$ is used; since each observation time is discretized to approximately 3 hours, this results in a total of about 9 hours of observation time to be allocated for each LET set during its approach to LLO. The field of view of an observer is set to FOV $= 60^\circ$. A total of $n_t = 101$ observation time steps are used for the observation horizon. With the $n_j = 703$ facilities from Table 2, the observation variables have dimensions $Y \in \mathbb{B}^{703}$ and $X \in \mathbb{B}^{5\times 703\times 200}$, resulting in 703703 binary variables in total. Despite the large number of variables, the binary formulation of the FLP is efficient to solve and takes 10s of seconds on the test desktop with 16 Intel i7-10700 CPUs and 32 GB of memory.

Three instances of the FLP with cut-off magnitude values of $m_{\text{co}} = 18$, 16, and 14 are considered. Note that a decreasing m_{co} corresponds to a tightening requirement since it requires the target to appear brighter to be visible to the observer. This is illustrated in the sparsity pattern of the visibility matrix M, as shown in Figure 5. For each LET set $i \in [1, \ldots, n_i]$, the plot shows the sparsity of $M_{i,:,:}$. Naturally, as the cut-off magnitude is decreased, the sparsity of M increases, resulting in less feasible allocations X_{ijt} that can satisfy the allocation constraint in (18). Compared with the families of LET in Figure 2, it is possible to associate LETs that are easier or harder to observe.

The solutions to the FLP for the three problem instances are summarized in Table 3. The phase, as given in the last column of the table, represents the initial phase of the observer as the fraction of the orbital period along the specific LPO at initial time $\theta_s = 0$. Note that $\theta_s = 0$ corresponds to when the Sun is on the x-axis of the Earth-Moon rotating frame, on the far side of the Moon. The corresponding architectures for each FLP instance are plotted in Figure 6. While for the two higher values of m_{co}, a single-observer spacecraft architecture is able to monitor the considered LET sets, the lowest m_{co} case requires three observer spacecraft. For this latter case, it is possible to see that the solution utilizes the 1:1 resonant Lyapunov orbit that passes through regions where the LETs loop on the L1 side.

For each solution, the resulting allocations are visualized in Figure 7. The angle in the polar plot corresponds to the Sun angle θ_s, where a full 360° corresponds to one synodic month. Each ring corresponds to an observer in the

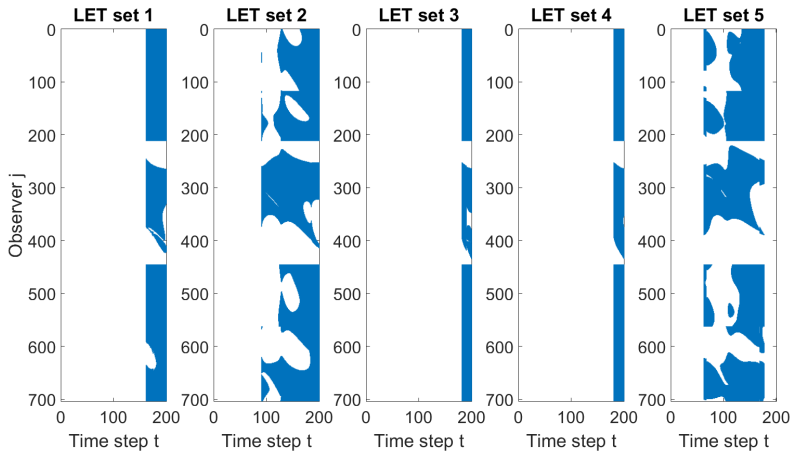

(a) $m_{\text{co}} = 18$

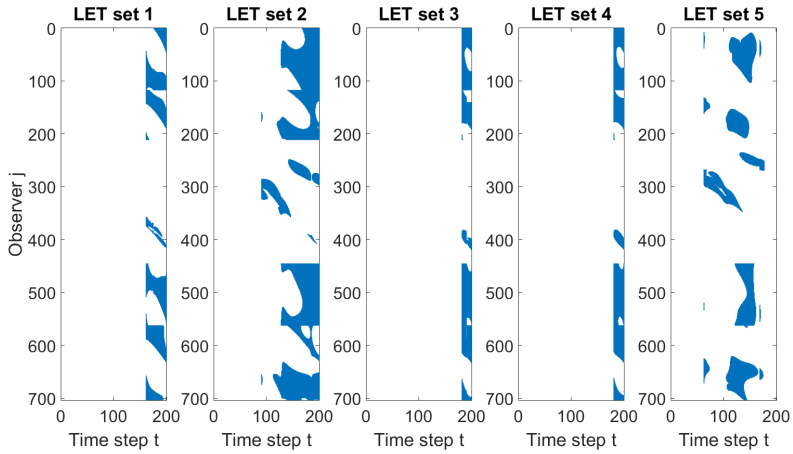

(b) $m_{\text{co}} = 16$

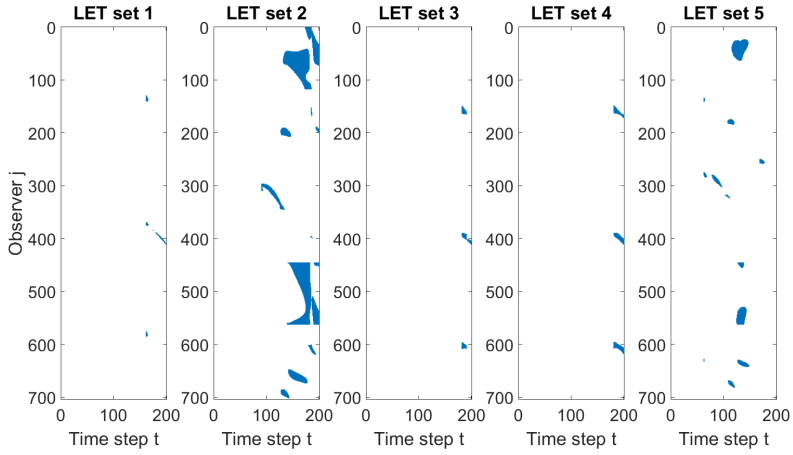

(c) $m_{\text{co}} = 14$

Fig. 5: Sparsity of visibility matrix M for each LET set at $m_{\text{co}} = 18$, 16, and 14. The sparsity is shown for each i, across $j \in \{1, n_j\}$ and $t \in \{1, n_t\}$.

Table 3: Observer locations chosen by instances of facility location problems with different values of m_{co}

Cut-off magnitude m_{co}	Number of observers	Observer locations (synodic resonance)	Phases
18	1	L2 Halo Southern (5:2)	0.7128
16	1	L2 Halo Southern (5:2)	0.1702
		L2 Halo Southern (5:2)	0.2128
14	3	L2 Halo Southern (5:2)	0.4574
		L2 Lyapunov (1:1)	0.4734

solution, and markers along the ring correspond to times (in terms of θ_s) where the observer is tasked with monitoring the region in space corresponding to the marker's LET set. Note that one revolution along θ_s corresponds to one period along the LPO only for a 1:1 resonance.

Observing the spread of the observation times, it is possible to see that observations most commonly occur as triplets, where subsequent or nearly subsequent observation opportunities are utilized to meet the required $N_{\Delta t}$ monitoring duration for a given LET set. For the $m_{co} = 14$ case, it is also possible to see that LET set 2 is observed by both L2 Halo observers, while the other LET sets are observed by either one of the three observers alone.

7. CONCLUSIONS

A monitoring architecture for LETs has been considered. The advantages of LETs make them a popular option for upcoming lunar exploration missions, which also translates to demands for being able to monitor spacecraft entering the lunar vicinity on a LET. Since the characteristically high apogees of LETs make them unsuitable to be monitored for large portions of the transfer, the SDA architecture is conceived to monitor LETs flying into the lunar vicinity from the L2 neck region.

In this work, a pre-computed database of LETs in the BCR4BP is used to cluster them into families, and an optimization problem to locate the minimal number of observer spacecraft to meet the monitoring requirement of these families is considered. The LETs are clustered in terms of both position and phase in order to collect transfers that can be observed through a single scan by the observer at a given time. The optimization problem is posed as a variant of the facility location problem (FLP), where a discretized set of slots along libration point orbits are considered as candidate locations for the observer spacecraft to be placed. The visibility of a cluster of LETs at each discretized time-step is considered by constructing the minimum-volume visibility sphere (MVVS), where all the LET states within the cluster are enclosed; the cluster is deemed to be visible if the least visible point within the MVVS is visible from the observer.

The proposed method is applied to a sample set of LETs, with various values of cut-off values on the maximum visible apparent magnitude. The FLP provides not only information on the number and location of the observer(s) but also the schedule where the observer should monitor a certain region in space where a cluster of LETs would pass through. The binary linear program nature of the FLP also makes it suitable for trade studies of system hyperparameters such as the observer's cut-off magnitude or field of view, as the solve time is on the order of seconds to minutes for the considered scale of the problem.

8. REFERENCES

[1] Gregory Badura, Yuri Shimane, Alaric Gregoire, Rohan Patel, Matthew Gilmartin, Kunal Gangolli, Lois Visonneau, Joshua Tysor, Saikrishna Manojkumar, Francis Humphrey, Chris Valenta, Reilly Blair, Nelson Lourenco, Jason Hodkin, Alicia Sudol, Mariel Borowitz, Brian Gunter, John Christian, and Koki Ho. System Design and Analysis for Cislunar Space Domain Awareness Through Distributed Sensors. In *AAS/AIAA Astrodynamics Specialist Conference*, pages 1–20, Charlotte, NC, 2022.

[2] Donald J Berndt and James Clifford. Using dynamic time warping to find patterns in time series. In *KDD workshop*, volume 10, pages 359–370. Seattle, WA, USA:, 1994.

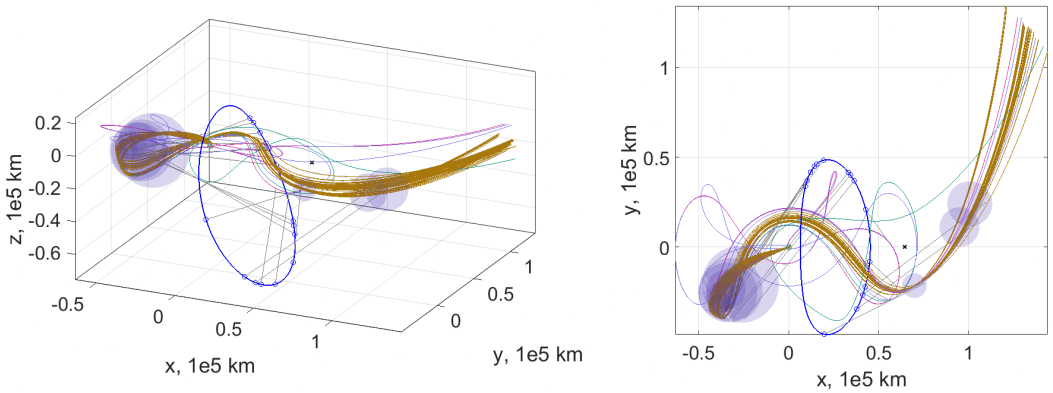

(a) $m_{\text{co}} = 18$

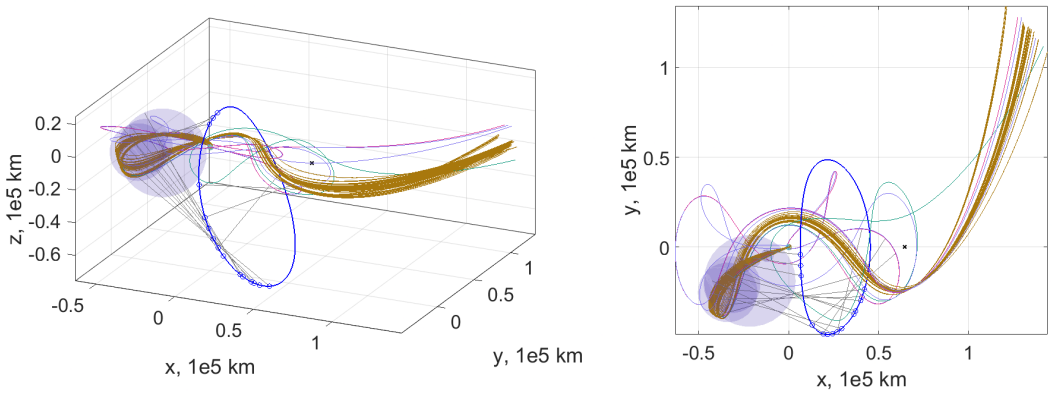

(b) $m_{\text{co}} = 16$

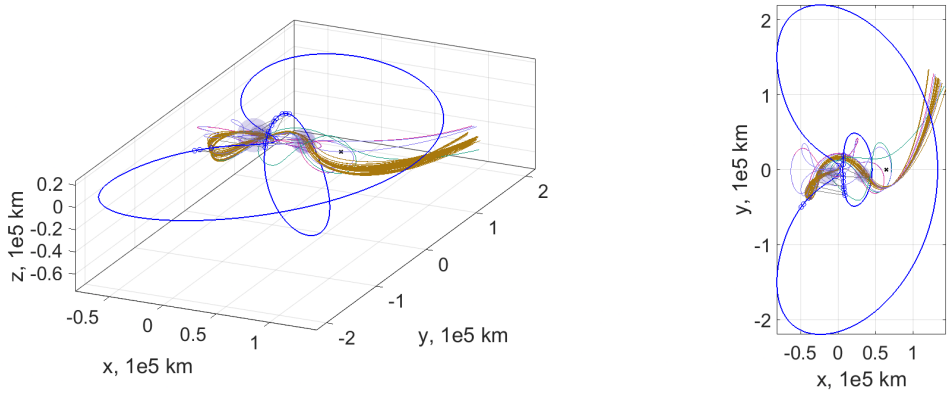

(c) $m_{\text{co}} = 14$

Fig. 6: Facility location problem solutions with $m_{\text{co}} = 18$, 16, and 14, shown in the Earth-Moon rotating frame centered at the Moon. The blue line indicates the observer's orbit, and the blue translucent spheres indicate the minimum-volume visibility sphere at time steps when the observation occurs.

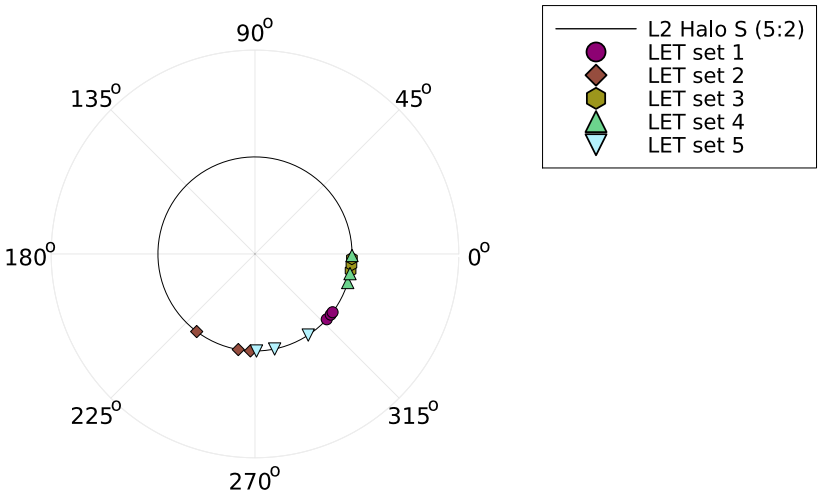

(a) $m_{\text{co}} = 18$

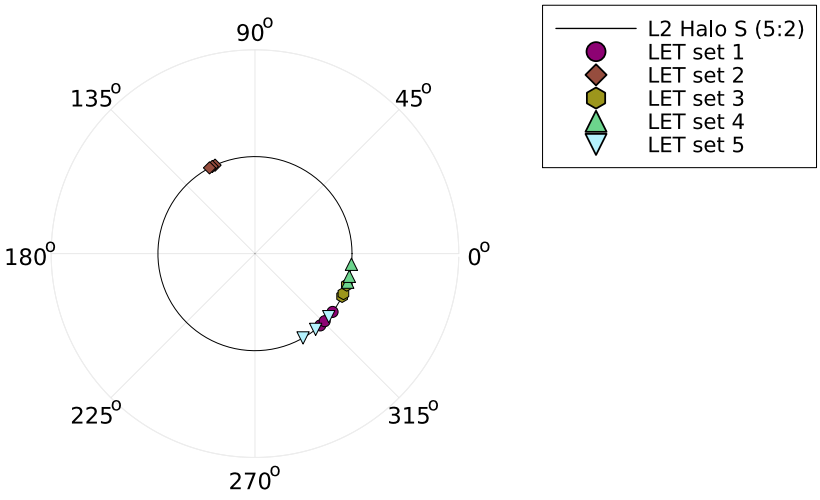

(b) $m_{\text{co}} = 16$

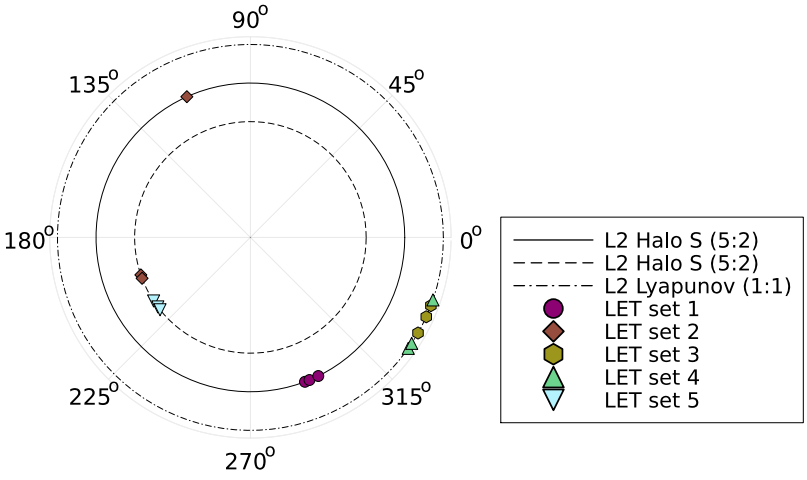

(c) $m_{\text{co}} = 14$

Fig. 7: Polar allocation plot of the solution from the facility location problem instances with $m_{\text{co}} = 18$, 16, and 14. The angle corresponds to the Sun angle θ_s, and the rings correspond to the three observers of the solution.

[3] Surabhi Bhadauria and Carolin Frueh. Optical Observation Regions in Cislunar Space Using the Bi-Circular Restricted Four Body Problem Geometry. In *Advanced Maui Optical and Space Surveillance Technologies (AMOS) Conference*, 2022.

[4] Mark Bolden, Timothy Craychee, and Erin Griggs. An evaluation of observing constellation orbit stability, low signal-to-noise, and the too-short-arc challenges in the cislunar domain. Maui, Hawai'i., 2020.

[5] Kenza K. Boudad, Kathleen C. Howell, and Diane C. Davis. Dynamics of synodic resonant near rectilinear halo orbits in the bicircular four-body problem. *Advances in Space Research*, 66(9):2194–2214, 2020.

[6] Bradley Cheetham, Thomas Gardner, Alec Forsman, Ethan Kayser, and Miekkal Clarkson. CAPSTONE: A Unique CubeSat Platform for a Navigation Demonstration in Cislunar Space. In *ASCEND 2022*, number October, pages 1–10, Reston, Virginia, oct 2022. American Institute of Aeronautics and Astronautics.

[7] Lei Chen, M Tamer Özsu, and Vincent Oria. Robust and fast similarity search for moving object trajectories. In *Proceedings of the 2005 ACM SIGMOD international conference on Management of data*, pages 491–502, 2005.

[8] Leon Cooper. Location-Allocation Problems. *Operations Research*, (December 2022), 1963.

[9] Gerard Cornuejols, Marshall L Fisher, and George L Nemhauser. Approximate Algorithms Linked references are available on JSTOR for this article : XeeptaDcetlna] Wap. *Management Science*, 23(8), 1977.

[10] Phillip M Cunio, Marcus J Bever, and Brien R Flewelling. Payload and constellation design for a solar exclusion-avoiding cislunar ssa fleet. Maui, Hawai'i., 2020. AMOS.

[11] Jacob A Dahlke, Adam P Wilmer, and Robert A Bettinger. Preliminary Comparative Assessment of L2 and L3 Surveillance Using Select Cislunar Periodic Orbits. In *AAS/AIAA Astrodynamics Specialist Conference*, pages 1–19, 2022.

[12] Phan Dao, Kristen Haynes, Victoria Frey, Cory Hufford, Kyle Schindler, Tamara Payne, and Jeffrey Hollon. Simulated photometry of objects in cislunar orbits. Maui, Hawai'i., 2020.

[13] Naomi Owens Fahrner, Jeremy Correa, and Joshua Wysack. Capacity-based Cislunar Space Domain Awareness Architecture Optimization Naomi Owens Fahrner Jeremy Correa Joshua Wysack. In *Advanced Maui Optical and Space Surveillance Technologies (AMOS) Conference*, 2022.

[14] Samuel Fedeler, Marcus Holzinger, and William Whitacre. Sensor tasking in the cislunar regime using monte carlo tree search. *Advances in Space Research*, 70:792–811, 8 2022.

[15] Erin E Fowler, Stella B Hurtt, and Derek A Paley. Orbit design for cislunar space domain awareness. 2020.

[16] C Frueh, K Howell, K J Demars, S Bhadauria, and M Gupta. Cislunar space traffic management: Surveillance through earth-moon resonance orbits. 2021.

[17] Gurobi Optimization, LLC. Gurobi Optimizer Reference Manual, 2022.

[18] S L Hakimi. Optimum Distribution of Switching Centers in a Communication Network and Some Related Graph Theoretic Problems. *Operations Research*, 13(3):462–475, 1965.

[19] Korea Aerospace Research Institute. Korea's first step toward lunar exploration.

[20] ispace. Hakuto-r mission 1. let's go to the moon.

[21] W. S. Koon, M. W. Lo, J. E. Marsden, and S. D. Ross. Low energy transfer to the Moon. *Celestial Mechanics and Dynamical Astronomy*, 81(1-2):63–73, 2001.

[22] Hang Woon Lee and Koki Ho. Regional Constellation Reconfiguration Problem: Integer Linear Programming Formulation and Lagrangian Heuristic Method. *Journal of Spacecraft and Rockets*, pages 1–18, jul 2023.

[23] Hang Woon Lee, Seiichi Shimizu, Shoji Yoshikawa, and Koki Ho. Satellite constellation pattern optimization for complex regional coverage. *Journal of Spacecraft and Rockets*, 57(6):1309–1327, 2020.

[24] Miles Lubin, Oscar Dowson, Joaquim Dias Garcia, Joey Huchette, Benoît Legat, and Juan Pablo Vielma. JuMP 1.0: Recent improvements to a modeling language for mathematical optimization. *Mathematical Programming Computation*, 2023.

[25] Pablo Machuca, Aaron J. Rosengren, and Shane D. Ross. xGEO Space Domain Awareness : Parametrization and Characterization of Cislunar Space Pablo Machuca , Aaron J . Rosengren Department of Mechanical and Aerospace Engineering , University of California San Diego , USA Shane D . Ross. In *Advanced Maui Optical and Space Surveillance Technologies (AMOS) Conference*, 2022.

[26] Jeffery S. Parker and Rodney L. Anderson. *Low-Energy Lunar Trajectory Design*. Wiley, Hoboken, New Jersey, 2014.

[27] Jeffrey S. Parker, Rodney L. Anderson, and Andrew Peterson. Surveying ballistic transfers to low lunar orbit. *Journal of Guidance, Control, and Dynamics*, 36(5):1501–1511, 2013.

[28] Malav Patel, Yuri Shimane, Hang Woon Lee, and Koki Ho. Cislunar Satellite Constellation Design via Integer Linear Programming. In *AAS/AIAA Astrodynamics Specialist Conference*, pages 1–18, 2023.

[29] Ralph Roncoli and Kenneth Fujii. Mission Design Overview for the Gravity Recovery and Interior Laboratory (GRAIL) Mission. In *AIAA/AAS Astrodynamics Specialist Conference*, number August 2010, pages 1–14, Reston, Virigina, aug 2010. American Institute of Aeronautics and Astronautics.

[30] Moshe B. Rosenwein. *Discrete location theory, edited by P. B. Mirchandani and R. L. Francis, John Wiley & Sons, New York, 1990, 555 pp*, volume 24. 1994.

[31] Yuri Shimane, Nick Gollins, and Koki Ho. Orbital Facility Location Problem for Satellite Constellation Servicing Depots. *arXiv*, 2023.

[32] David "Simchi-Levi, Xin Chen, and Julien" Bramel. *The Logic of Logistics*. Springer, New York, 2014.

[33] Yaguang Tao, Alan Both, Rodrigo I Silveira, Kevin Buchin, Stef Sijben, Ross S Purves, Patrick Laube, Dongliang Peng, Kevin Toohey, and Matt Duckham. A comparative analysis of trajectory similarity measures. *GIScience & Remote Sensing*, 58(5):643–669, 2021.

[34] Michael R Thompson, Nathan P Ré, Cameron Meek, and Bradley Cheetham. Cislunar orbit determination and tracking via simulated space-based measurements. Maui, Hawai'i., 2021.

[35] Jacob K. Vendl and Marcus J. Holzinger. Cislunar Periodic Orbit Analysis for Persistent Space Object Detection Capability. *Journal of Spacecraft and Rockets*, 58(4):1174–1185, 2021.

[36] Lois Visonneau, Yuri Shimane, and Koki Ho. Optimizing Multi-Spacecraft Cislunar Space Domain Awareness Systems via Hidden-Genes Genetic Algorithm. *The Journal of the Astronautical Sciences*, 2023.

[37] Emo Welzl. Smallest enclosing disks (balls and ellipsoids). In Hermann Maurer, editor, *New Results and New Trends in Computer Science*, pages 359–370, Berlin, Heidelberg, 1991. Springer Berlin Heidelberg.

[38] Adam P Wilmer and Robert A Bettinger. Near-Rectilinear Halo Orbit Surveillance using Cislunar Periodic Orbits. In *Advanced Maui Optical and Space Surveillance Technologies (AMOS) Conference*, 2022.

[39] Adam P. Wilmer, Robert A. Bettinger, and Bryan D. Little. Cislunar periodic orbits for earth–moon l1 and l2 lagrange point surveillance. *Journal of Spacecraft and Rockets*, 11 2022.

[40] Gert W. Wolf. Facility location: concepts, models, algorithms and case studies. series: Contributions to management science. *International Journal of Geographical Information Science*, 25(2):331–333, 2011.

[41] Andreas Wächter and Lorenz T. Biegler. On the implementation of an interior-point filter line-search algorithm for large-scale nonlinear programming. *Mathematical Programming*, 106(1):25–57, 2005.